Trans. Japan Soc. Aero. Space Sci.
Vol. 65, No. 1, pp. 33–43, 2022
DOI: 10.2322/tjsass.65.33

Study on the Ignition Method for n-Octane Pyrolysis Fuel in a Scramjet Engine*

Shinichiro OGAWA,[1)†] Kan KOBAYASHI,[2)] and Sadatake TOMIOKA[2)]

[1)]*Department of Aerospace Engineering, Tohoku University, Sendai, Miyagi 980–8579, Japan*
[2)]*Kakuda Space Center, Japan Aerospace Exploration Agency, Kakuda, Miyagi 981–1525, Japan*

In scramjet engines, ignition must take place within a residence time on the order of milliseconds. In this study, secure ignition conditions for specified n-octane pyrolysis fuel components used in autoignition or forced-ignition by plasma jet torch in a high-speed flow were numerically investigated. First, the ignition delay time within the combustor and cavity flame-holder was estimated using chemical reaction analysis. Three fuel components (n-C_8H_{18}, all pyrolysis fuel (15 components, decomposition rate under 11%)), and pyrolysis gas fuel (eight gas fuel components, decomposition rate under 11%) could not self-ignite within the combustor and cavity residence time. Secondly, ignition using a plasma jet torch in the cavity was numerically investigated. In the case of forced-ignition by plasma jet torch, all pyrolysis fuel (No. 3) and n-C_8H_{18} could ignite within the cavity residence time with less input energy than pyrolysis gas fuel (No. 3) under three kinds of Mach number flight conditions ($M_0 = 4$, 6, and 8). Moreover, the effect of shortening the ignition delay time by raising the plasma jet torch gas temperature and O radical rate within the cavity was investigated. Ignition of the three kinds of mixture fuel was more greatly affected by the torch injection temperature than the O radical rate in the cavity under all Mach number flight conditions.

Key Words: Ignition Delay Time, Plasma Jet, Chemical Reaction Analysis, Scramjet Engine, Internal Flows

Nomenclature

A: area
D: cavity depth
F: temperature recovery factor
M: Mach number
$\dot{m}$: mass flow rate
P_{IN}: input power
p: pressure
R: ideal gas constant
T: temperature
U: main flow
X: mole fraction
$\tau_{res.}$: residence time
σ: shear layer growth parameter
σ^*: critical flow coefficient
β: Zeldovich number
γ: specific heat ratio
Ω_k: collision integral
Φ: equivalence ratio

Subscripts

b: uniform
cavity: cavity condition
comb.: combustor condition
fuel/air: fuel/air mixture
I: ionization
m: distributed
mix: mixture
PJ_gas: injection gas from the PJ torch
R: recirculation zone
t: total
w: wall

1. Introduction

The scramjet engine has attracted widespread interest in fields such as hypersonic vehicles. Many research institutions have been investigating the scramjet engine.[1,2)] At the Japan Aerospace Exploration Agency (JAXA), a practical flight experiment using a scramjet engine has been explored, and a flight test system utilizing a sounding rocket is planned.[3)] Downsizing of the fuel tank is an important factor for realizing flight test models and hypersonic vehicles. For example, much research in recent years has focused on scramjet engines using hydrocarbon fuels.[4–6)] Hydrocarbon fuel is selected as a propellant for good packing into airplane-like vehicle shapes because the fuel tank becomes compact in size.[5)] Hydrocarbon liquid fuel at room temperature has an advantage that an integral tank can be incorporated in the hypersonic vehicle. However, hydrocarbon fuel has a disadvantage in that it has lower cooling and ignition capabilities. To solve the problem of poor cooling capability, an additional cooling capability through endothermic reactions by thermal cracking is expected to be effective. The endothermic reaction of kerosene-based fuels was achieved at fuel exit temperatures above 700°C, and it can be implemented using conventional kerosene-based fuels as the heat sink.[7)] Furthermore, fuel coking in the cooling channel oc-

*Presented at the 32nd International Symposium on Space Technology and Science, 15–21 June 2019, Fukui, Japan
Received 2 November 2020; final revision received 18 April 2021; accepted for publication 14 June 2021.
†Corresponding author, ogawa@scrj.mech.tohoku.ac.jp

curs at a high temperature. The coking rate is expected to be high in aircraft fuel systems.[8)]

The scramjet engine cycle from cooling to ignition is as follows. The heavy hydrocarbon fuel (e.g., n-dodecane, Jet A-1) inside the fuel tank runs in the cooling passage, consequently cooling the engine via the endothermic reactions generated by thermal cracking. The turbine is driven by hydrocarbon pyrolysis fuels (i.e., fuel after thermal cracking) that are heated in the cooling passage. After that, the pyrolysis fuel, which includes various hydrocarbon fuels, is injected into a supersonic crossflow from the orifice. This is a regenerative cooling system, and JAXA has proposed using a regenerative cooling system in scramjet engines.[9)]

To combust the pyrolysis fuel in a scramjet engine, it is necessary to solve two important autoignition problems in the engine. The first autoignition problem is the short residence time of airflow in engine. The residence time is on the millisecond order from fuel orifice to nozzle exit.[10)] The second autoignition problem is that the pyrolysis fuel contains a component that results in long ignition delay time. The ignition delay time differs based on the hydrocarbon fuel components.[11)] For example, because the larger liquid parent fuel decomposes into smaller gaseous hydrocarbons at high temperature, it is anticipated that these changes in the fuel state or chemical composition will significantly alter the fuel injection behavior and the subsequent ignition and combustion process.[12,13)]

Previous research investigated the supersonic combustion of hydrocarbon pyrolysis fuels such as n-dodecane,[14)] kerosene,[12)] and jet fuel.[15)] Nakaya et al. evaluated the supersonic combustion of a surrogate fuel of the n-dodecane pyrolysis fuel which had four components (i.e., hydrogen, methane, ethane, and ethylene). Moreover, they investigated the combustion effect of adding hydrogen, methane, and ethylene to basic fuel 1 (6% H_2/29% CH_4/23% C_2H_6/41% C_2H_4).[14)] Fan et al. conducted an autoignition test of cracked kerosene in a Mach 2.5 model combustor using a range of fuel injection conditions and varying amounts of pilot hydrogen.[12)] From the experimental results, they indicated that the amount of pilot hydrogen required for achieving autoignition decreased as the extent of kerosene cracking increased.[12)] Nakayama et al. investigated the combustion characteristics of jet fuel and pyrolysis fuel (subcritical condition and supercritical condition) in the ramjet/scramjet mode. From the experimental results, in the scramjet mode, although the fuel cracking rates in the tests-firings were different, the wall pressure distributions were almost identical.[15)] However, they indicated that the influence of fuel cracking on the combustion characteristics could not be investigated quantitatively, and the investigation was limited to a qualitative discussion.[15)] The detailed ignition characteristics of all pyrolysis components were not clarified because previous research had only been carried out to investigate pyrolysis gas components.

Many researchers have investigated forced-ignition using the plasma jet torch method[16–20)] in scramjet engines. Takita et al. numerically and experimentally investigated the suitability of plasma ignition for hydrocarbon fuels in high-speed flows.[18–20)] They investigated the effect of radicals using three kinds of plasma jet (PJ) feedstock (O_2, N_2, and Ar). From the results of the study, for fuel injection both upstream and downstream of the PJ, the three PJ feedstocks showed no difference with respect to the location and behavior of ignition.[18)] However, flames ignited using the N_2 PJ and Ar PJ blew out while the O_2 PJ held the flame after ignition.[18)] It was clear that the O_2 PJ held the flame after ignition because the O_2 gas remaining in the torch was injected into the combustor. Moreover, Takita et al. investigated the ignition and flame-holding characteristics of methane, propane, and hydrogen in the case of different PJ torch igniter locations.[19,20)] Ignition and combustion of methane, propane, and hydrogen fuels occurred more easily for fuel injection upstream of the PJ torch than for injection downstream of the PJ torch.[19,20)] In addition, ignition of the methane fuel was confirmed only when the PJ torch gas was injected upstream of the torch.[20)] These results indicate that the local O_2 concentration around the ignition site is very important for successfully enhancing ignition and combustion in a high-speed flow.[19)] Based on previous studies, secure ignition conditions using forced-ignition with a PJ jet torch for thermally cracked hydrocarbon fuel could not be clarified. To ignite thermally cracked components of hydrocarbon fuel using a PJ torch, it is necessary to survey the effects of torch injection gas conditions (i.e., torch injection gas temperature, torch injection gas component, and radical) for ignition.

The purpose of this study is to propose a secure ignition method for the specified n-octane pyrolysis fuel components, from autoignition or forced-ignition using a PJ torch, in scramjet engines. In this study, the ignition delay time is estimated using zero-dimensional chemical reaction analysis. The calculation conditions for the ignition delay time corresponded to the flight Mach numbers of 4–8. n-Octane was selected in this study because it is a surrogate fuel for aviation gasoline. Aviation gasoline is containing of over 50% (by weight) molecules that contain eight carbon atoms.[8)] As a preliminary step to study the ignition of aviation gas, the authors investigated the ignition of n-octane, which has a simpler reaction process than aviation gas. In addition, many researchers have studied the reaction model of n-octane, and a reaction model suitable for the ignition delay time of n-octane has been constructed. Furthermore, there is sufficient data on thermal cracking experiments regarding n-octane.[21)]

Ignition in the scramjet engine was investigated in terms of autoignition within the combustor and cavity and forced ignition using the PJ torch. The three fuel components were n-octane single component, pyrolysis gas fuel (eight gas fuel components), and all pyrolysis fuels (15 components including liquid components). The research process for the scramjet engine was as follows: Step 1, autoignition within the combustor and cavity internal flow; and Step 2, forced ignition using the PJ torch. The target engine was the JAXA E2R,[22)] and combustion experiments were conducted using this engine at the JAXA-Ramjet Engine Test Facility (RETF). The residence time (combustor and cavity), static

pressure, and static temperature in the scramjet engine were calculated. In this study, the calculation conditions for ignition delay time during flights at Mach 4–8 were a static pressure of 0.1 MPa and a static temperature of 500–1200 K. The feedstock gas of the PJ torch was oxygen.

2. Analysis Method

2.1. Research process flow

In this section, the research process flow is explained. In the present investigation of ignition in scramjet engines, three scramjet engine internal conditions were the focus: (A) fuel component, (B) combustor and cavity internal flow, and (C) PJ torch. Figure 1 shows the research process flow in this study. The goal of this process is to recommend a secure ignition method for pyrolysis fuel. In this study, three fuel cases with different components are utilized: n-octane single component, pyrolysis gas fuel (eight gas fuel components), and all pyrolysis fuels (15 components including liquid components). Firstly, the autoignition of three fuel components at combustor and cavity internal flow conditions were investigated. Secondly, if autoignition failed, forced ignition using a PJ torch in the cavity was investigated. All ignition studies were performed with flow conditions simulating flight at Mach 4–8.

As previously informed, there are three fuel case components: n-octane single component, pyrolysis gas fuel (only gas fuel consisting of the eight components of H_2, CH_4, C_2H_4, C_2H_6, C_3H_6, C_3H_8, i-C_4H_8, and n-C_4H_{10}), and all pyrolysis fuel components (consisting of H_2, CH_4, C_2H_4, C_2H_6, C_3H_6, C_3H_8, i-C_4H_8, n-C_4H_{10}, i-C_5H_{10}, n-C_5H_{12}, i-C_6H_{12}, n-C_6H_{14}, i-C_7H_{14}, n-C_7H_{16}, and n-C_8H_{18}). The n-C_8H_{18} single component was a fuel that has not been pyrolyzed.

The thermal cracking experiment data of Miyaura et al.[21] was used in this study. A flow reactor with a heater at the Kakuda Space Center of JAXA was used for the n-octane thermal cracking experiment. The experimental equipment was composed of a preheating section and heating section. Moreover, the heating section was composed of two section heaters, and the fuel was heated while being supplied. The thermal cracking experiment conditions were as follows: residence time of 0.43–0.52 s, fuel temperature in the downstream part of the heater of 792–935 K, and the pressure was 6.0 MPa. n-Octane was heated up to a supercritical condition to facilitate thermal cracking. The n-octane thermal cracking experiment data are shown in Fig. 2. Case 1 was with a fuel temperature of 729 K and a decomposition rate of 2.5%. Case 2 was with a fuel temperature of 823 K and a decomposition rate of 4.6%. Case 3 was with a fuel temperature of 935 K and a decomposition rate of 11.1%. From the thermal-cracking component data, it was found that methane, ethylene, ethane, and propane were the main components of the pyrolysis fuel. Moreover, the cracking component had a high percentage of alkane in components over C_3. In this study, the ignition characteristics of premixed fuel (pyrolysis fuel or n-C_8H_{18}/air) were investigated using this composition.

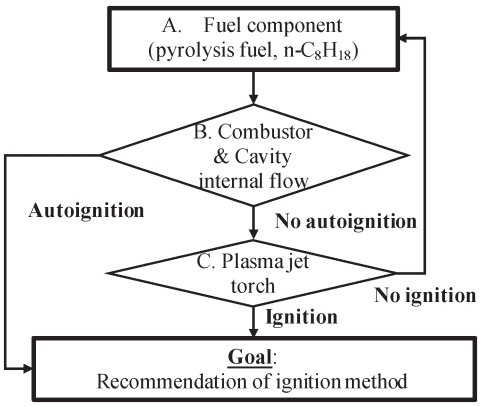

Fig. 1. Research process flow in this study.

2.2. Chemical analysis and reaction model

All simulations were performed using closed homogeneous modules in the CHEMKIN-PRO package[23] assuming constant-volume and adiabatic (CONV) conditions. The closed homogeneous module was a zero-dimensional chemical reaction analysis code. The constant-volume and adiabatic conditions have often been used in the chemical reaction analysis of ignition delay time.[24]

The definition of ignition delay time varies depending on the researchers. Huber et al.[25] and Pergament[26] defined that ignition was accomplished when the temperature rise reached 5% of the complete reaction temperature rise. Mével et al.[27] and Spadaccini et al.[28] defined that ignition was accomplished at the time when OH emission peaked. In this study, the ignition time was defined as the time when the OH radical reached the maximum value.

The Knowledge-based Utilities for Complex Reaction System (KUCRS) model[29,30] and JetSurF 2.0 model[31] were used for the reaction mechanism to calculate the ignition delay time. Table 1 shows the reaction model information: number of elements, species, and reactions. The KUCRS model is a utility software library for the development of gas-phase chemical kinetic models of hydrocarbon oxidation or combustion reaction system.[29] The JetSurF 2.0 model was

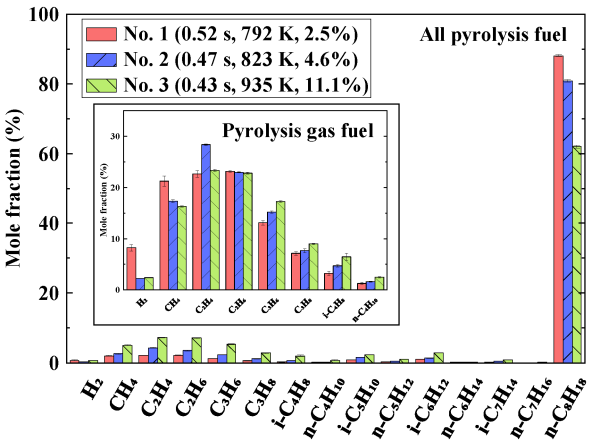

Fig. 2. The thermal-cracking component data of n-octane at three different fuel temperatures in the downstream part of the heater.[16]

Table 1. Chemical reaction model information.

	Elements	Species	Reactions
KUCRS	6	123	977
JetSurF 2.0	6	348	2164

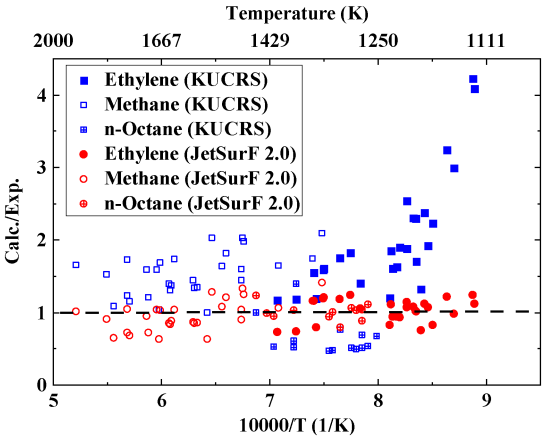

Fig. 3. Validation analysis results of the n-octane, methane, and ethylene single component using the KUCRS and JetSurF 2.0 models.

Table 2. Average Calc./Exp. of KUCRS and JetSurF 2.0 models.

	$n\text{-}C_8H_{18}$	CH_4	C_2H_4
KUCRS	0.74	1.53	2.02
JetSurF 2.0	1.00	0.96	1.03

developed by the Wang Group, and this model is a detailed chemical reaction model for the combustion of jet-fuel surrogates.[31)]

The chemical reaction models were verified by comparison with the ignition experiment data. Objects of the validation analysis were n-octane, methane, and ethylene single components. The reason for choosing the methane and ethylene was that the thermally cracked liquid hydrocarbon fuel (kerosene, n-dodecane, etc.) contain a large fraction of methane and ethylene.[32)] Figure 3 shows the validation analysis results. The validation results for n-octane were compared with the experimental data of Davidson et al.,[24)] the validation analysis results for methane were compared with the experimental data of Spadaccini et al.,[28)] and the validation analysis results for ethylene were compared with the experimental data of Colket et al.[11)] On the vertical axis, the calculation data were normalized with experiment data (Calc./Exp.). Calc./Exp. = 1.0 indicates that the analysis results are identical to the experimental datum. Table 2 shows the average Calc./Exp. for the KUCRS model and JetSurF 2.0 model for $n\text{-}C_8H_{18}$, CH_4, and C_2H_4. The results of the KUCRS model indicate that there was a different gradient between the calculation data and experimental data on the low-temperature side from 1100–1250 K. On the other hand, the calculation data of the JetSurF 2.0 model shows similarities to experimental data for all conditions. Therefore, the JetSurF 2.0 model was used in this study.

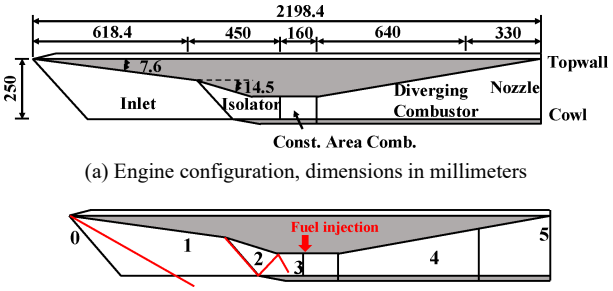

(a) Engine configuration, dimensions in millimeters

(b) Engine internal conditions in five calculation areas

Fig. 4. Engine model based on a JAXA E2R engine.

3. Autoignition Characteristics in the Combustor and Cavity

3.1. Combustor internal flow conditions

The object of calculation for combustor internal flow conditions was a scramjet engine model based on the JAXA E2R,[22)] as shown in Fig. 4. The E2R engine had a ramp block that fully covers the top wall. The total length of the engine was 2198.4 mm. At the entrance of the inlet, the heights of the internal ducts were 250 mm. In this study, the width of the engine was fixed at 70 mm. As shown in Fig. 4(a), the block had two ramps with different angles at the inlet and isolator section. The first lamp was at an angle of 7.6 deg to the engine axis, and the subsequent second ramp was at an angle of 14.5 deg. The engine internal conditions were calculated for five areas (see Fig. 4(b)). The five calculation areas were as follows: area 0–3 were from the inlet entrance to the combustor, area 4 was the combustor, and area 5 was the nozzle exit.

A combustor internal flow study was performed for flight conditions of Mach 4, 6, and 8. Firstly, the combustor entrance conditions between areas 0–3, as shown in Fig. 4(b), were calculated. Area 0 is in the freestream flow ahead of the vehicle. Area 1 is downstream of the shock wave from the engine leading-edge. Area 2 is the inlet throat. Area 3 is the constant area combustion, and fuel was added in this area. The air inside the scramjet inlet was compressed through a series of oblique shock waves. Hence, four oblique shock waves were calculated using the oblique shock wave equation.[33)] To simplify calculation of the combustor entrance conditions, the following assumption was made: friction forces or heat transfer to/from the wall were nonexistent. Secondly, the combustor residence time ($\tau_{res\_comb.}$) was calculated based on the Heiser and Pratt equation.[34)] The combustor residence time was estimated using the length between the fuel orifice and nozzle exit (1130 mm). In this study, non-combustion conditions are assumed for calculating the combustor residence time. Table 3 shows the calculation results for engine internal conditions at flight conditions of Mach 4–8. Additionally, autoignition is extremely sensitivity to the mixture temperature at the pertinent ignition location.[25)] For example, wall temperature and recirculation zone temperature recovery factors have a dominant influence on the autoignition phenomenon.[25)] In this study, the recircu-

Table 3. The internal flow conditions at flight speeds of Mach 4–8.

	$M_0 = 4$	$M_0 = 6$	$M_0 = 8$
Freestream conditions			
Z_0 [km]	22	27	31
V_0 [m/s]	1184.6	1798.1	2417.7
P_0 [kPa]	4.28	1.90	1.07
T_0 [K]	218	223	227
Combustor entrance (Station 3)			
V_3 [m/s]	875.60	1387.32	1904.49
M_3	2.01	2.63	3.04
P_3 [kPa]	65.9	77.4	95.0
P_{3t} [kPa]	428.2	655.1	954.9
T_3 [K]	484	707	997
T_{3t} [K]	836	1591	2663
Nozzle (Station 5)			
V_5 [m/s]	1118.4	1684.8	2241.6
T_5 [K]	323	404	475
$\tau_{res\_comb.}$ [ms]	1.111	0.715	0.538

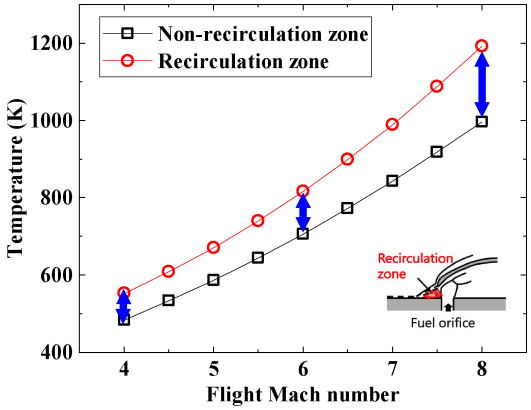

Fig. 5. The combustor internal temperature conditions of the recirculation and non-recirculation zones at flight conditions of Mach 4–8.

lation zone temperature in front of the fuel jet was estimated based on a model of Huber et al.[25] The recirculation zone temperature T_R was calculated as

$$T_R = F_R(T_t - T_w) + T_w \tag{1}$$

where T_R is the recirculation zone temperature, F_R is the recirculation zone temperature recovery factor, T_t is the total temperature of the main flow, and T_w is the wall temperature. For a Reynolds number of around 10^6, the value of F_R from approximately 0.3–0.7 was given for wall-temperature ratios T_w/T_t from about 0.1–0.6.[25] In this study, the F_R was 0.35, and the T_w was 400 K.[25] Figure 5 shows the recirculation zone temperature at the flight conditions of Mach 4–8. The initial conditions for chemical reaction analysis were set as follows: initial static pressure of 0.1 MPa and initial static temperature of 500–1200 K.

3.2. Cavity internal flow conditions

In the case that the pyrolysis fuel does not self-ignite in the combustor, autoignition conditions in the cavity were investigated. The mass exchange between the vortices inside the cavity is relatively small, and therefore, as the trailing-edge vortex occupies a large volume inside the cavity, the mass exchange increases and flow residence time inside the cavity decreases.[35] In the combustion experiment of scramjet mode

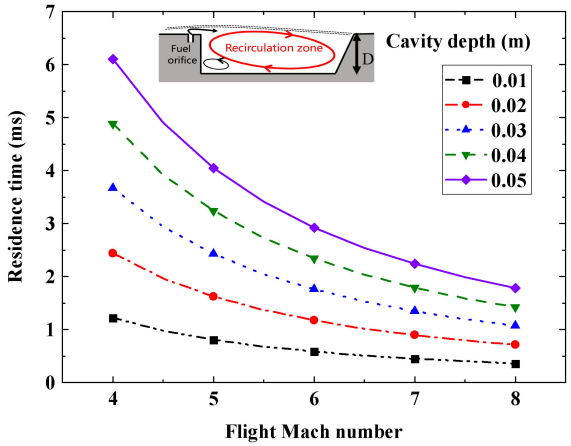

Fig. 6. The residence time at different cavity depths: $D = 0.01$, 0.02, 0.03, 0.04, and 0.05 m.

operation using jet fuel, a peak in the wall pressure was observed around the aft end of the cavity; hence, it was deduced that the exothermic chemical reaction peaked.[15]

The cavity residence time τ_{res_cavity} was estimated based on the model of Davis and Bowersox.[36] It was derived using the cavity depth D and the velocity of the main flow U,

$$\tau_{res\_cavity} = \frac{7.1\sigma}{1 + \dfrac{\gamma - 1}{2}M^2} \cdot \frac{D}{U} \tag{2}$$

where M is the Mach number, γ is the specific heat ratio, and σ is the shear layer growth parameter. The shear layer growth parameter σ varies from 13 to 30 depending on the convective Mach number.[36] For example, the shear layer growth parameter σ was approximately 27 at $M = 2.0$.[36] The residence time in the cavity was calculated for five cavity depths (0.01, 0.02, 0.03, 0.04, and 0.05 m). Figure 6 shows the residence time at different cavity depths.

3.3. Results and discussion regarding autoignition conditions

In this section, the ignition delay times for the three previously described premixed-fuel conditions were numerically analyzed to determine whether or not thermal cracking affected the ignition delay time, and if it did, how. The premixed fuel-air equivalence ratio was 1.0. From the plot of the Ozawa curve,[37] which correlates the blowout limits of premixed subsonic flames, the equivalence ratio 1.0 is easier for holding flame after ignition than other equivalence ratios.[38] Therefore, an equivalence ratio of 1.0 is used for discussion in this section. The combustor internal flow conditions discussed in Section 3.1 and the cavity internal flow conditions discussed in Section 3.2 are also used in this section. The ignition delay time of the premixed pyrolysis gas fuel, all of the pyrolysis fuels, and n-C_8H_{18} at a static temperature and the pressure of the main flow are shown in Fig. 7. The red line is the residence time in the combustor ($\tau_{res\_comb.}$), and the blue lines are the residence time in the cavity (τ_{res_cavity}). The blue lines show the residence time at different cavity depths: the chain double-dashed line is a depth of $D = 0.01$ m, the chain line is a depth of $D =$

0.02 m, the dotted line is a depth of $D = 0.03$ m, the broken line is a depth of $D = 0.04$ m, and the solid line is a depth of $D = 0.05$ m.

The ignition delay time of all fuels exhibited a systematic decrease as the temperature increased. The ignition delay time difference due to the difference in decomposition rate was investigated for all pyrolysis fuels and pyrolysis gas fuels, respectively. Comparing No. 1 (decomposition rate of 2.5%) and No. 3 (decomposition rate of 11.1%), which revealed a large difference in the thermal decomposition rate among the three cases, the maximum difference in ignition delay time at 1100 K was 8.8%. Moreover, in the case of pyrolysis gas fuels, the maximum difference in ignition delay time at 1200 K was 20.9%. The difference in ignition delay time due to the difference in the decomposition rate of all the pyrolysis fuels was small. However, the ignition delay time difference was large for the pyrolysis gas fuels. The reason for the small ignition delay time difference for all of the pyrolysis fuels was that the hydrocarbon fuel (e.g., C_2H_4), which has good ignitability, had a small impact on the ignition of all pyrolysis fuels because, even in the case of No. 3, which has a high decomposition rate, it was composed of 89% n-C_8H_{18}. Moreover, the all-pyrolysis fuels showed the same ignition delay time as n-C_8H_{18}.

On the high-temperature side, where ignition is easy, the all-pyrolysis fuels (No. 3), which had a high decomposition rate, showed the best ignition characteristics. However, as shown in Fig. 7, under the condition of $\varphi = 1.0$, there was no autoignition of the all-pyrolysis fuels when attempting to ignite within the combustor and cavity residence time. Therefore, forced ignition using the PJ torch method was required to ignite the fuel. Therefore, forced ignition using the PJ torch method is investigated in the next section. Furthermore, in the following ignition studies, only No. 3 (decomposition rate of 11.1%) was used among the three conditions of the decomposition rate. The reason for using No. 3 was that the No. 3 all-pyrolysis fuels has a shorter ignition delay time than the other decomposition rate conditions in the entire range of initial temperatures.

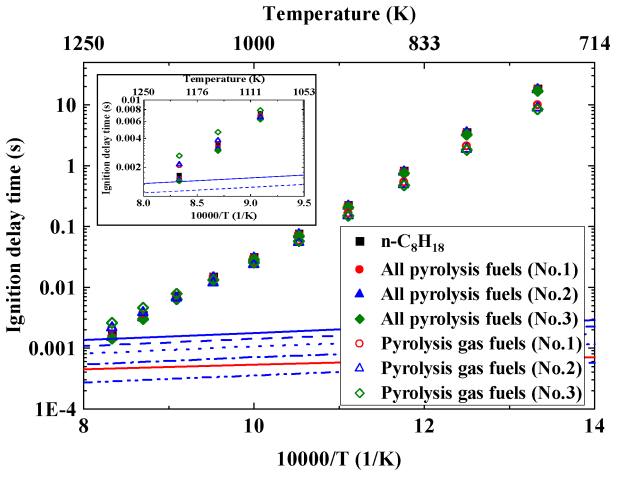

Fig. 7. Arrhenius plot of n-C_8H_{18}, all-pyrolysis fuels, and pyrolysis gas fuel ignition delay times, $\varphi = 1.0$. The red line is $\tau_{res\_comb.}$, and the blue line is τ_{res_cavity}.

4. Ignition Characteristics under Torch-lit Conditions

4.1. PJ torch conditions

The PJ torch is well-known to drastically shorten ignition delay due to the existence of a small amount of radicals.[17,18,39] Therefore, in the case of a pyrolysis fuel not being able to self-ignite in the combustor and cavity, promoting pyrolysis fuel ignition using a PJ torch was investigated. In this study, the PJ torch was the same as that used in the experiments conducted by Takita et al.[39] The diameter of the nozzle throat was 1.5 mm and the flow rate of the PJ was set at 0.33 g/s. Takita et al.[39] investigated the effect of radicals using the three kinds of PJ feedstock gas (O_2, N_2, and Ar). From the results of this study, for fuel injection both upstream and downstream of the PJ, the three PJ feedstock gases revealed no difference with respect to the location and behavior of ignition.[18] Therefore, in this study, oxygen was selected as the feedstock gas for the PJ torch.

The PJ torch injection conditions were estimated based on a calculation method of Kobayashi et al.[40] Figure 8 shows the schematic diagram of the PJ torch injection conditions in the cavity. In this study, the PJ torch was installed at the bottom of the cavity. The cavity has a front step height of 20 mm and a close-out ramp angle of 30 deg. The cavity is characterized by a length-to-depth ratio L/D of 5. In this study, uniform temperature and the O radical are assumed.

The uniform temperature T_b was defined as follows:

$$T_b = \frac{4}{\beta_I} \frac{\Gamma\left(\frac{3}{2}, \frac{\beta_I}{4} T_{w(gas)}\right) - \Gamma\left(\frac{3}{2}, \frac{\beta_I}{4}\right)}{\Gamma\left(\frac{1}{2}, \frac{\beta_I}{4} T_{w(gas)}\right) - \Gamma\left(\frac{1}{2}, \frac{\beta_I}{4}\right)} \tag{3}$$

where β_I is the ionization Zeldovich number ($\equiv T_I/T_m$), and $T_{w(gas)}$ is the gas temperature at the wall. The gas temperature at the wall was fixed at 1000 K. The reason for fixing at 1000 K is that the PJ injection nozzle is made of copper and copper has a melting point of 1360 K.

The stagnation pressure of the PJ torch was calculated from the mass flow rate equation for isenthalpic flow.

$$\dot{m} = \sigma^* \cdot p_t \cdot A/\sqrt{R \cdot T_t} \tag{4}$$

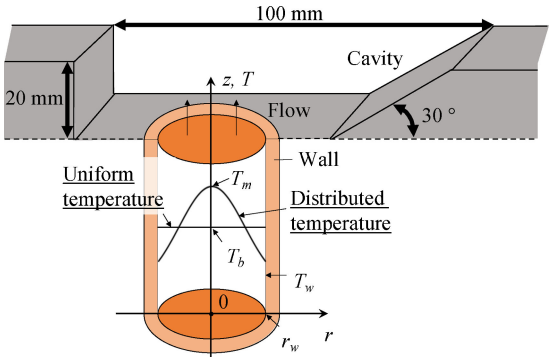

Fig. 8. Schematic diagram of PJ torch injection conditions in the cavity.

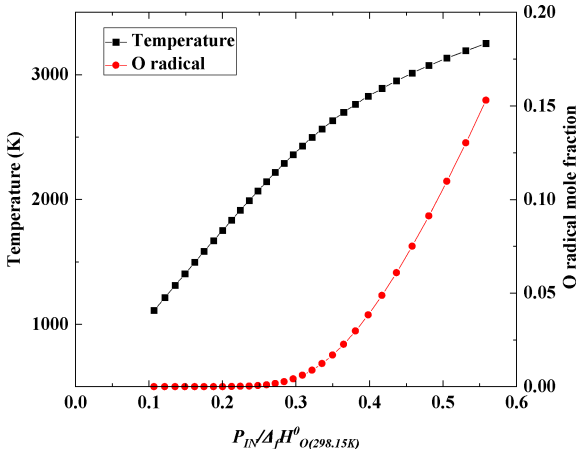

Fig. 9. Uniform temperature and O radical production under PJ torch injection conditions against electrical power input.

The composition of the PJ exhaust was estimated using the CEA code[41] developed by NASA. The chemical equilibrium computation was repeated so that the error between the mass flow rate and set flow rate (0.33 g/s) was less than 1.0%.

The uniform temperature and O radical production of the PJ torch against electric power input are shown in Fig. 9. The input energy delivered to the PJ torch is defined as the summation of two kinds of energy: thermal and chemical.[40] The thermal energy is the sensible heat. Therefore, the thermal energy was defined as the energy that contributed to the temperature rise of the working gas. Chemical energy was defined as the Gibbs free energy.[40] The thermal energy can be estimated from the temperature of the PJ. The chemical energy can be estimated from the radical concentration and its enthalpy of formation. The two kinds of energy were estimated using the Joint Army-Navy-Air Force (JANAF) table.[42] The horizontal axis is the dimensionless value of the input energy resulting from the enthalpy of O radical formation ($\Delta_f H^0{}_{O\ (298.15\,\mathrm{K})} = 249.17\,\mathrm{kJ/mol}$). The uniform temperature changed between 1000–3000 K, with $P_{IN}/\Delta_f H^0{}_{O\ (298.15\,\mathrm{K})} = 0.1$–$0.55$. The O radical was generated with a $P_{IN}/\Delta_f H^0{}_{O\ (298.15\,\mathrm{K})}$ of 0.19.

The torch gas component and the temperature in the cavity at the time of torch gas injection were calculated. To simplify the calculation of the torch gas ratio and temperature in the cavity, several assumptions were made: 1) the torch gas was a steady flow, and 2) the gas inside the cavity was completely replaced within the cavity residence time. Firstly, the mass flow rate of the fuel/air mixture gas flowing into the cavity was calculated from the volume flow rate and density, where the volume flow rate was calculated from the volume of the cavity and the cavity residence time. The cavity residence time was estimated using Eq. (2). Next, the torch gas ratio in the cavity was calculated from the mass flow rate of the fuel/air mixture gas flowing into the cavity and the mass flow rate of PJ torch gas. Table 4 shows the torch gas ratio in the cavity under flight conditions of Mach 4, 6, and 8. The torch gas ratio in the cavity was defined as the mass flow ratio of the torch gas and cavity gas. The torch

Table 4. Torch gas ratio in the cavity under flight conditions of Mach 4, 6, and 8.

	All-pyrolysis fuels (No. 3)	Pyrolysis gas fuels (No. 3)	n-C_8H_{18}
$M_0 = 4$	0.24%	0.25%	0.24%
$M_0 = 6$	0.14%	0.15%	0.14%
$M_0 = 8$	0.10%	0.10%	0.10%

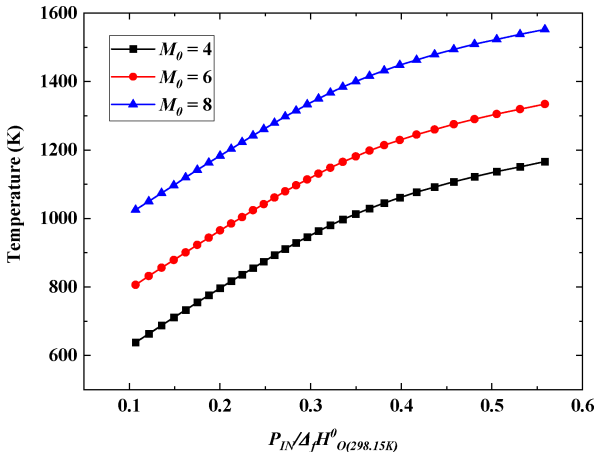

Fig. 10. Temperature in the cavity at the time of torch gas injection.

gas ratio in the cavity was 0.24–0.25% under the flight condition of Mach 4, 0.14 to 0.15% under the flight condition of Mach 6, and 0.10% under the flight condition of Mach 8. The temperature in the cavity at the time of torch gas injection was estimated based on a calculation model for a mixture temperature presented by Huber et al.[25] The mixture temperature was defined as follows:

$$T_{mix} \approx T_{fuel/air} - \frac{0.327\Phi}{1 + 0.327\Phi}(T_{fuel/air} - T_{PJ\_gas}) \quad (5)$$

where $T_{fuel/air}$ is the fuel/air mixture gas temperature and T_{PJ_gas} is the injection gas temperature from the PJ torch. Figure 10 shows the temperature in the cavity at the time of torch gas injection. At $P_{IN}/\Delta_f H^0{}_{O\ (298.15\,\mathrm{K})} = 0.10$–$0.55$, the temperature in the cavity at the time of torch gas injection was 600–1100 K under the flight condition of Mach 4, 800–1300 K under the flight condition of Mach 6, and 1000–1500 K under the flight condition of Mach 8. The initial component of the PJ torch was as follows. The O radical was 0.0–0.15% mole, and the oxygen was 0.85–1.0% mole.

4.2. Results and discussion regarding forced ignition using the PJ torch

The numerical results were verified with the experimental results of ignition limits measured experimentally by Kobayashi et al.[40,43] A rectangular combustor with rearward-facing steps was adopted. Mach number, total temperature, and total pressure of the airflow were 2.5, 800–2500 K, and 1.0 MPa, respectively. The main fuel was gaseous hydrogen at room temperature. The feedstock gas of PJ torch was oxygen. The feedstock gas flow rates of PJ torch were 5–10 l/min. The residence time for the downstream step

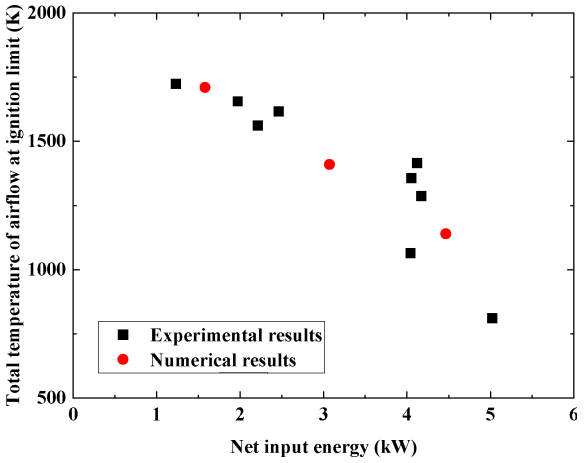

Fig. 11. Comparison of experimental data and calculation data in the case of airflow total temperature at ignition limit.

was estimated using the model of Zakkay et al.[44] Figure 11 shows the comparison with experimental data and calculation data in the case of total airflow temperature at the ignition limit. From the validated results, the numerical results of this study showed an equivalent gradient to the experimental results of ignition limits for forced ignition using a PJ torch.

Figure 12 shows the variation in ignition delay time against the input power at $P_{IN}/\Delta_f H^0{}_{O\ (298.15\,\mathrm{K})} = 0.1$–$0.55$. The ignition delay time was calculated for the three different hydrocarbon fuels mentioned previously. The decomposition ratio of the pyrolysis gas fuels (No. 3) and all-pyrolysis fuels (No. 3) was 11.1%. The cavity residence time was used in this section because the PJ torch was installed at the bottom of the cavity. Residence times at a cavity depth 0.02 m for flight conditions of Mach 4, 6, and 8 were estimated using Eq. (2). The ignition delay time of the three kinds of fuel mixture exhibited a decrease as input power increased, and this was because the uniform temperature and O radical production rate increased. Table 5 shows the input energy ($P_{IN}/\Delta_f H^0{}_{O\ (298.15\,\mathrm{K})}$) when hydrocarbon fuel could ignite within the residence time at a cavity depth 0.02 m under flight conditions of Mach 4, 6, and 8.

The non-decomposed condition (n-C_8H_{18}) and the decomposed conditions (all-pyrolysis fuels and pyrolysis gas fuels) were compared to determine which had better ignition when applying the forced ignition method using a PJ torch. Firstly, n-C_8H_{18} and the all-pyrolysis fuels (No. 3) were compared to determine the input energy required for ignition within the residence time at a cavity depth of 0.02 m. The input energy differences where ignition was possible within the cavity residence time were 3.8% under the flight condition of Mach 4, 2.2% under the flight condition of Mach 6, and 1.4% under the flight condition of Mach 8. It was clear that there is no difference in forced ignition between n-C_8H_{18} and the all-pyrolysis fuels (No. 3) when using the PJ torch. Therefore, in the case of forced ignition using a PJ torch, there is no advantage of ignitability for the all-pyrolysis fuels (No. 3) with a decomposition rate under 11.1%.

Next, n-C_8H_{18} and pyrolysis gas fuels (No. 3) were compared to determine which had better ignitability when applying the forced ignition method using a PJ torch. At the time of low-energy input, the ignition delay time of the pyrolysis gas fuels (No. 3) was shorter than the ignition delay time of n-C_8H_{18}. On the other hand, this trend was reversed at the time of high-energy input. For example, the changing point where the ignition delay times of n-C_8H_{18} and the pyrolysis

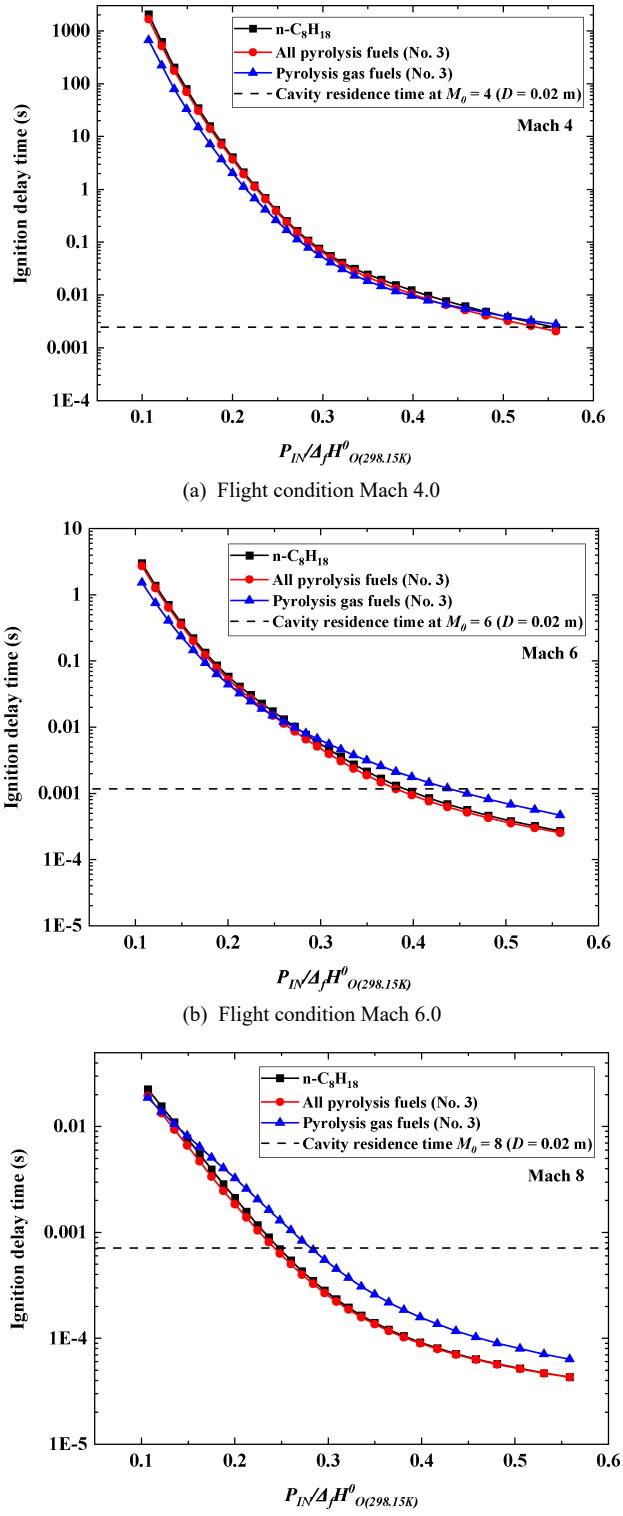

(a) Flight condition Mach 4.0

(b) Flight condition Mach 6.0

(c) Flight condition Mach 8.0

Fig. 12. The variation in ignition delay time for the input power of PJ torch.

Table 5. Input energy ($P_{IN}/\Delta_f H^0{}_{O\ (298.15\,K)}$) when hydrocarbon fuel could ignite within the residence time at a cavity depth of 0.02 m under flight conditions of Mach 4, 6, and 8.

	All-pyrolysis fuels (No. 3)	Pyrolysis gas fuels (No. 3)	n-C_8H_{18}
$M_0 = 4$	0.555	0.609	0.576
$M_0 = 6$	0.323	0.458	0.330
$M_0 = 8$	0.212	0.284	0.215

Table 6. Temperature and O radical rate in the cavity when hydrocarbon fuel could be ignited within the residence time at a cavity depth of 0.02 m and flight condition of Mach 4, 6, and 8.

	All-pyrolysis fuels (No. 3)	Pyrolysis gas fuels (No. 3)	n-C_8H_{18}
Mach 4.0			
T_{cavity} [K]	1154	1180	1164
X_{O_cavity} [mol%]	0.038	0.051	0.044
Mach 6.0			
T_{cavity} [K]	1215	1275	1223
X_{O_cavity} [mol%]	0.006	0.011	0.007
Mach 8.0			
T_{cavity} [K]	1252	1315	1259
X_{O_cavity} [mol%]	7.83E−5	0.0003	0.0001

gas fuels reversed was $P_{IN}/\Delta_f H^0{}_{O\ (298.15\,K)} = 0.51$ under the flight condition of Mach 4, $P_{IN}/\Delta_f H^0{}_{O\ (298.15\,K)} = 0.28$ under the flight condition of Mach 6, and $P_{IN}/\Delta_f H^0{}_{O\ (298.15\,K)} = 0.15$ under the flight condition of Mach 8. The input energy difference, when ignition was possible within the cavity residence time, was 5.7% under the flight condition of Mach 4, 38.8% under the flight condition of Mach 6, and 32.1% under the flight condition of Mach 8. Therefore, in the case of forced ignition using the PJ torch, n-C_8H_{18} has better ignitability than the pyrolysis gas fuels. It was clear that the all-pyrolysis fuels (No. 3) and n-C_8H_{18} can be ignited within the cavity residence time using less energy input than pyrolysis gas fuels (No. 3) under the three kinds of Mach flight conditions.

The feed fuel component for the combustor varies depending on the operating conditions of the engine. For example, when the engine is started, the temperature inside the engine is low and thermal decomposition has not occurred in the cooling passage. In this case, n-octane is supplied to the combustion chamber. Therefore, when the engine is started, we expect that the fuel was easily forced to ignite using the PJ torch, because n-octane has better forced-ignition performance than the pyrolysis gas fuels. In the future, from the engine system study, the best fuel supply method in terms of ignition and cooling needs to be investigated.

The effect of shortening the ignition delay time using PJ torch gas temperature and O radical rate within the cavity was investigated. Table 6 shows the temperature and O radical rate in the cavity when hydrocarbon fuel could ignite within the residence time at a cavity depth of 0.02 m and flight conditions of Mach 4, 6, and 8. Figure 13 shows the effect of radical ratio from the PJ torch on ignition promotion within the cavity at 1200 K. At the flight condition of Mach 8, all three kinds of fuel mixture can be ignited using small

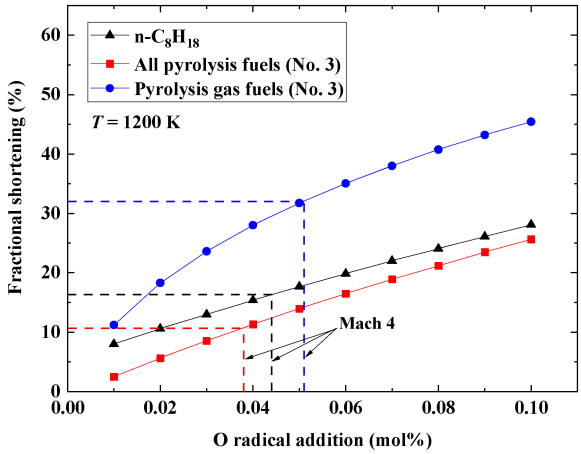

Fig. 13. Effects of radical ratio from PJ torch on ignition promotion within the cavity at 1200 K.

energy input (shown in Table 5). This is because the initial temperature in the cavity (no injection of torch gas) under the flight condition of Mach 8 was higher than other Mach flight conditions. Therefore, under the flight condition of Mach 8, a comparison between the fractional shortening of the ignition delay time due to the radical concentration and that due to the torch injection temperature showed that the torch injection temperature had higher fractional shortening than the radical concentration. For example, as shown in Fig. 13, when the O radical rate was 3×10^{-4} mol% or less, the fractional shortening due to O radicals was 10% or less and had little influence on ignition. This result was the same under the flight condition of Mach 6.

At the flight condition of Mach 4, a comparison between the fractional shortening of the ignition delay time due to the radical concentration and that due to the torch injection temperature showed that the torch injection temperature had higher fractional shortening than the radical concentration. However, as shown in Table 6, the temperature in the cavity was 1200 K or less, and from the results of autoignition (see Section 3.3), there was no autoignition condition that could ignite within the cavity residence time at 1200 K. Therefore, assuming the same temperature (1200 K), the ignition promoting effect of adding O radicals was investigated. As shown in Fig. 13, the fractional shortening of the ignition delay time due to the O radical addition rate was found in the descending order of pyrolysis gas fuels > n-C_8H_{18} > all-pyrolysis fuels. It was clear that the fuel mixture which was difficult ignite using autoignition had a greater ignition promoting effect due to the addition of O radicals. For example, from the data in Table 6, when 0.038 mol% of O radicals was added to the all-pyrolysis fuels (No. 3), the shortening rate was 11% (ignition delay time difference of 0.016 ms). On the other hand, when 0.051 mol% of O radicals was added to the pyrolysis gas fuels (No. 3), the shortening rate was 32% (ignition delay time difference of 0.837 ms). According to the above results in this study, under the flight condition of Mach 4, where the initial temperature in the cavity (no injection torch gas) is lower than other Mach

flight conditions, not only the torch gas temperature, but also the O radical addition rate slightly affected the ignition delay time.

5. Conclusion

The purpose of this study was to propose a secure ignition method for specified n-octane pyrolysis fuel components in scramjet engines under the condition of autoignition or forced ignition using a plasma jet torch. The results are summarized as follows:

1) In the case of autoignition characteristics in the combustor and cavity, under the condition of $\varphi = 1.0$, there is no ignition condition in which all of the fuel mixtures ignite within the combustor and cavity residence time. Therefore, a method requiring forced ignition using a plasma jet torch is required to ignite the pyrolysis fuels.

2) Comparing the results of n-C_8H_{18} and all-pyrolysis fuels (No. 3) in the case of forced ignition using a plasma jet torch, there was no advantage for ignitability for the all-pyrolysis fuels (No. 3), which had a decomposition rate of under 11.1%. This is because there is no difference in ignition between n-C_8H_{18} and all-pyrolysis fuels (No. 3) when applying forced ignition using the plasma jet torch.

3) In the case of forced ignition using the plasma jet torch, the all-pyrolysis fuels (No. 3) and n-C_8H_{18} can both ignite within the cavity residence time using less energy input energy than the pyrolysis gas fuels (No. 3) under all three kinds of Mach flight conditions.

4) Ignition of the three kinds of fuel mixtures was more greatly affected by the torch injection temperature than the O radical rate in the cavity for all Mach flight conditions. However, at the flight condition of Mach 4, where the initial temperature in the cavity (no injection torch gas) is lower than the other Mach flight conditions, not only the torch gas temperature, but also the O radical addition rate slightly affect the ignition delay time.

The authors calculated the ignition delay time assuming that the fuel in the combustor and cavity is a premixed fuel. However, the fuel is not completely premixed in an actual engine. In addition, the heat transfer to the cooling channels changes depending on the combustion condition in the combustor. The mixing ratio of hydrocarbon fuel in thermally cracked hydrocarbon fuel changes accordingly. Therefore, the ignition delay time was calculated based on assumptions, and the ignition limit of the thermally cracked hydrocarbon fuel in the scramjet engine was estimated theoretically.

In the future, in the case of thermally cracked hydrocarbon fuels, the calculation results used for ignition experiments involving scramjet combustors should be validated. In addition, from the engine system study, investigation of the best fuel supply method in terms of ignition and cooling is required. Furthermore, the flame holding mechanisms after the ignition of pyrolysis fuels remains to be determined. Future work should be focused on the flame-holding mechanisms of pyrolysis fuels in scramjet engines.

References

1) Moses, R. L., Rausch, V. L., Nguyen, L. T., and Hill, J. R.: NASA Hypersonic Flight Demonstrators—Overview, Status, and Future Plans, *Acta Astronautica*, **55** (2004), pp. 619–630.
2) Hank, J. M., Murphy, J. S., and Mutzman, R. C.: The X-51A Scramjet Engine Flight Demonstration Program, AIAA Paper 2008-2540, 2008.
3) Tani, K., Onodera, T., Kato, K., and Takegoshi, M.: Flight Experiment for the Validation of New Methodology to Compensate the Wind Tunnel Contamination Problem, Proceedings of 32nd International Symposium on Space Technology and Science, 2019-m-11, June 2019.
4) Powell, O. A., Edwards, J. T., Norris, R. B., Numbers, K. E., and Pearce, J. A.: Development of Hydrocarbon-Fueled Scramjet Engines: The Hypersonic Technology (HyTech) Program, *J. Propul. Power*, **17** (2001), pp. 1170–1176.
5) Tomioka, S., Hiraiwa, T., Saito, T., Kato, K., Kodera, M., and Tani, K.: System Analysis of a Hydrocarbon-Fueled RBCC Engine Applied to a TSTO Launch Vehicle, *Trans. JSASS Aerospace Technology Japan*, **12** (2014), pp. Pa_91–Pa_99.
6) Ueda, S., Tomioka, S., Saito, T., Tani, K., and Yoshida, M.: R&D on Hydrocarbon-fueled RBCC Engines for a TSTO Launch Vehicle, AIAA Paper 2015-3611, 2015.
7) Huang, G., Spadaccini, L. J., and Sobel, D. R.: Fuel-Cooled Thermal Management for Advanced Aeroengines, *J. Eng. Gas Turbines Power*, **126** (2004), pp. 284–293.
8) Edwards, T.: Liquid Fuels and Propellants for Aerospace Propulsion: 1903–2003, *J. Propul. Power*, **19** (2003), pp. 1089–1107.
9) Kanda, T., Masuya, G., and Wakamatsu, Y.: Propellant Feed System of a Regeneratively Cooled Scramjet, *J. Propul. Power*, **7** (2012), pp. 299–301.
10) Mauris, L., Edwards, T., and Griffiths, J.: Liquid Hydrocarbon Fuels for Hypersonic Propulsion, *Scramjet Propulsion*, AIAA, Virginia, 2001, pp. 757–822.
11) Colket, M. B. and Spadaccini, L. J.: Scramjet Fuels Autoignition Study, *J. Propul. Power*, **17** (2001), pp. 315–323.
12) Fan, X., Yu, G., Li, J., Lu, X., Zhang, X., and Sung, C. J.: Combustion and Ignition of Thermally Cracked Kerosene in Supersonic Model Combustors, *J. Propul. Power*, **23** (2007), pp. 317–324.
13) Tishkoff, J. M., Drummpmd, J. P., Edwards, T., and Nejad, A. S.: Future Direction of Supersonic Combustion Research: Air Force/NASA Workshop on Supersonic Combustion, AIAA Paper 97-1017, 1997.
14) Nakaya, S., Tsue, M., Kono, M., Imamura, O., and Tomioka, S.: Effects of Thermally Cracked Component of n-Dodecane on Supersonic Combustion Behaviors in a Scramjet Model Combustor, *Combustion Flame*, **162** (2015), pp. 3847–3853.
15) Nakayama, H., Edanaga, T., Hashino, S., Tomioka, S., Kobayashi, K., and Takahashi, M.: A Dual-mode Scramjet Combustor Employing a Jet Fuel for Hypersonic Flight Vehicle, AIAA Paper 2018-4452, 2018.
16) Sato, Y., Wakamatsu, Y., Ohwaki, K., Masuya, G., Komuro, T., Kudou, K., Murakami, A., Tani, K., Wakamatsu, Y., Kanda, T., Chinzei, N., and Kimura, I.: Effectiveness of Plasma Torches for Ignition and Flameholding in Scramjet, *J. Propul. Power*, **8** (1992), pp. 883–889.
17) Mitani, T.: Ignition Problems in Scramjet Testing, *Combustion Flame*, **101** (1995), pp. 347–359.
18) Takita, K.: Ignition and Flame-holding by Oxygen, Nitrogen and Argon Plasma Torches in Supersonic Airflow, *Combustion Flame*, **128** (2002), pp. 301–313.
19) Takita, K., Ohashi, R., and Abe, N.: Suitability of C2-, C3-Hydrocarbon Fuels for Plasma Ignition in High-Speed Flow, *J. Propul. Power*, **25** (2009), pp. 565–570.
20) Kitagawa, T., Moriwaki, A., Murakami, K., Takita, K., and Masuya, G.: Ignition Characteristics of Methane and Hydrogen Using a Plasma Torch in Supersonic Flow, *J. Propul. Power*, **19** (2003), pp. 853–858.
21) Miyaura, T., Shimuta, A., Daimon, Y., and Tomioka, S.: Study on Chemical Heat Sink of Liquid Hydrocarbon under Supercritical Condition, Proceedings of Space Transportation Symposium FY2017, STCP-2017-020, January 2018 (in Japanese).
22) Hiraiwa, T., Kobayashi, K., and Saito, T.: Experiments on Scramjet Engine, with Ramp-Compression Inlet at Mach 8, *J. Propul. Power*,

22 (2006), pp. 440–446.
23) ANSYS CHEMKIN-Pro, Software Package, Ver. 19.2, ANSYS, Canonsburg, PA, 2019.
24) Davidson, D. F. and Hanson, R. K.: Interpreting Shock Tube Ignition Data, *Int. J. Chem. Kinet.*, **36** (2004), pp. 510–523.
25) Huber, P. W., Schexnayder, C. J., Jr., and McClinton, C. R.: Criteria for Self-Ignition of Supersonic Hydrogen-Air Mixtures, NASA TM-1457, 1979.
26) Pergament, H.: A Theoretical Analysis of Non-Equilibrium Hydrogen-Air Reactions in Flow Systems, AIAA Paper 1963-113, 1963.
27) Mével, R. and Shepherd, J. E.: Ignition Delay-time behind Reflected Shock Wave of Small Hydrocarbons-nitrous Oxide (-oxygen) Mixture, *Shock Waves*, **25** (2015), pp. 217–229.
28) Spadaccini, L. J. and Colket, M. B., III: Ignition Delay Characteristics of Methane Fuels, *Prog. Energy Combust. Sci.*, **20** (1994), pp. 431–460.
29) Miyoshi, A.: KUCRS (Knowledge-Basing Utilities for Complex Reaction Systems), KUCRS Software Library, http://akrmys.com/KUCRS/ (accessed November 10, 2018).
30) Miyoshi, A.: Systematic Computational Study on the Unimolecular Reactions of Alkylperoxy (RO_2), Hydroperoxyalkyl (QOOH), and Hydroperoxyalkylperoxy (O_2QOOH) Radicals, *J. Phys. Chem. A*, **115** (2011), pp. 3301–3325.
31) Wang, H., Dames, E., Sirjean, B., Sheen, D. A., Tango, R., Violi, A., Lai, J. Y. W., Egolfopoulos, F. N., Davidson, D. F., Hanson, R. K., Bowman, C. T., Kaw, C. K., Tsang, W., Cernansky, N. P., Miller, D. L., and Lindstedt, R. P.: JetSurF Version 2.0, Chemical Reaction Model Database, http://web.stanford.edu/group/haiwanglab/JetSurF/JetSurF2.0/index.html (accessed November 10, 2018).
32) Fan, X., Zhong, F. Q., Yu, G., Li, G., and Sung, C. J.: Catalytic Cracking and Heat Sink Capacity of Aviation Kerosene under Supercritical Conditions, *J. Propul. Power*, **25** (2009), pp. 1226–1232.
33) Anderson, J. D., Jr.: Oblique Shock and Expansion Waves, *Modern Compressible Flow with Historical Perspective*, 3rd ed., McGraw-Hill, New York, 2003, pp. 127–190.
34) Heiser, W. H. and Pratt, D. T.: Hypersonic Airbreathing Engine Performance Analysis, *Hypersonic Airbreathing Propulsion*, AIAA, Washington D. C., 1994, pp. 149–196.
35) Ben-Yakar, A. and Hanson, R. K.: Cavity Flame-Holders for Ignition and Flame Stabilization in Scramjets: An Overview, *J. Propul. Power*, **17** (2001), pp. 869–877.
36) Davis, D. L. and Bowersox, R. D. W.: Stirred Reactor Analysis of Cavity Flame Holders for Scramjets, AIAA Paper 97-3274, 1997.
37) Ozawa, R. I.: Survey of Basic Data on Flame Stabilization and Propagation for High Speed Combustion Systems, AFAPL Technical Rept. TR-70-81, 1971.
38) Driscoll, J. F. and Rasmussen, C. C.: Correlation and Analysis of Blowout Limits of Flame in High-Speed Airflows, *J. Propul. Power*, **21** (2005), pp. 1035–1044.
39) Takita, K., Moriwaki, A., Kitagawa, T., and Masuya, G.: Ignition and Flame-holding of H_2 and CH_4 in High Temperature Airflow by a Plasma Torch, *Combustion Flame*, **132** (2003), pp. 679–689.
40) Kobayashi, K., Tomioka, S., and Mitani, T.: Supersonic Flow Ignition by Plasma Torch and H_2/O_2 Torch, *J. Propul. Power*, **20** (2004), pp. 294–301.
41) Gordon, S. and McBride, B. J.: Computer Program for Calculation of Complex Chemical Equilibrium Compositions and Applications I. Analysis, NASA RP-1311, 1994.
42) Chase, M. W., Jr., Davies, C. A., Downey, J. R., Jr., Frurip, D. J., McDonald, R. A., and Syverud, A. N.: JANAF Thermochemical Tables Third Edition, *J. Phys. Chem. Ref. Data*, **14** (1985), Supplement No. 1.
43) Masuya, G., Kudo, K., Murakami, A., Komuro, T., Tani, K., Kanda, T., Wakamatsu, Y., Chinzei, N., Sayama, M., Ohwaki, K., and Kimura, I.: Some Governing Parameters of Plasma Torch Igniter/Flameholder in a Scramjet Combustor, *J. Propul. Power*, **9** (1993), pp. 176–181.
44) Zakkay, V., Sinha, R., and Medecki, H.: Residence Time within a Wake Recirculation Region in an Axisymmetric Supersonic Flow, AIAA Paper 70-111, 1970.

Toru Shimada
Associate Editor